Near-Wall Modelling of Compressible Turbulent Flows

by

Ronald M.C. So
Mechanical and Aerospace Engineering
Arizona State University
Tempe, Arizona

A Semi-Annual Progress Report Submitted

to

September 1, 1990

Summary

This progress report summarizes the work carried out during the period January 1 to June 30, 1990. During this period, work has been carried out to extend the near-wall models formulated for the incompressible Reynolds-stress equations to compressible flows. The idea of splitting the compressible dissipation function into a solenoidal part that is not sensitive to changes of compressibility indicators and a compressible part that is directly affected by these changes is adopted. This means that all models involving the dissipation rate could be expressed in terms of the solenoidal dissipation rate and an equation governing its transport could be formulated to close the set of compressible Reynolds-stress equations. The near-wall modelling of the dissipation-rate equation is investigated and its behavior near a wall is studied in detail using a k-ε closure. It is found that all existing modelled equations give the wrong behavior for the dissipation rate near a wall. Improvements are suggested and the resultant behavior is found to be in good agreement with near-wall data. Furthermore, the present modified k-ε closure is used to calculate a flat plate boundary layer and the results are compared with four existing k-ε closures. These comparisons show that all closures tested give essentially the same flow properties, except in a region very close to the wall. In this region, the present k-ε closure calculations are in better agreement with measurements and direct simulation data; in particular, the behavior of the dissipation rate.

Contents

1. Introduction

Density variation in a turbulent flow can come from different origins. Some of these are: (i) isothermal mixing of gases of different density, (ii) strong temperature gradient in a homogeneous fluid, (iii) reactive flows and (iv) compressibility effects in high speed flows. Each of these origins gives rise to specific aspects that require modelling if the governing flow equations are to be solved. This project makes an attempt to address the last origin; that is, the modelling of high speed compressible turbulent flows.

Most studies on turbulent compressible flow modelling [1-5] invoke the Morkovin postulate [6] to justify the direct extension of the incompressible models to compressible flows. The postulate was formulated based on early experiments on compressible boundary layers along adiabatic walls and compressible wakes, and essentially suggested that the dynamical field in a compressible flow behaves like an incompressible one. This postulate was used by numerous researchers to assure that compressibility effects can be accounted for correctly by the variable mean density in the governing equations alone. The validity and extent of Morkovin's postulate was reviewed by Bradshaw [2] and he noted that the postulate is appropriate for flows where the density fluctuations are moderate. Therefore, the postulate is not valid for hypersonic boundary layers, where the Mach number is five or greater, and for flows with strong pressure gradient effects, such as shock-turbulent-boundary-layer interactions. The latter point was confirmed by the studies of Wilcox and Alber [1] and Bradshaw [7] and led to proposals to have the effects of pressure-dilatation correlation modelled in the governing equations [8]. Besides this modification, all turbulent compressible flow modelling rely on incompressible models. Therefore, their applicability is limited.

Two sources of difficulties arise when incompressible turbulence models are extended to compressible flows. One is due to compressibility itself and another is associated with the turbulence phenomena. In the case of compressible flows, the flow equations are coupled and

temperature can no longer be considered as a passive scalar. Rather, it is an active scalar and all other thermodynamic variables play new roles as a result. Therefore, mathematically, compressible flows cannot be considered as straightforward extension of incompressible flows. Furthermore, pressure is only a force term in incompressible flows and all disturbances propagate at infinite speed. On the other hand, pressure also supports finite velocity propagation of disturbances in compressible flows. Further complications come from the variable mean density, which contributes to increased non-linearity of the governing equations, and the fluctuating density, which causes the closure problem to become more difficult.

The second source of difficulties has to do with the turbulence phenomena. Here, even for incompressible flows, many problems remain to be resolved [9,10], especially when the flow is unsteady and/or three-dimensional [11]. However, among the many problems associated with turbulence modelling, one stands out as most fundamental and urgently needs attention. This is the treatment of the near-wall flow. Conventional approach is to invoke the wall function assumption; thus implying that the turbulence is in local equilibrium. Even for simple shear flows, the assumption is not quite valid because near-wall turbulence is not in local equilibrium. Consequently, a near-wall treatment is necessary in order to obtain results that agree with measurements in the near-wall region [12,13,14]. The need for near-wall treatment of flows with heat and mass transfer has also been pointed out [15,16]. This problem, therefore, is expected to be more acute in compressible turbulent flow modelling. In this case, as pointed out above, temperature cannot be considered as a passive scalar and the variable mean density further compounds the non-linearity of the governing equations. The present project attempts to model near-wall compressible turbulent flow where there is a strong coupling between velocity and temperature.

2

2. Review of the modelling of incompressible near-wall flows

With the advent of high-speed computers, it is widely accepted that the isotropic diffusivity and wall function approach has to be abandoned for the calculation of complex turbulent flows [9-18]. This is especially the case for heat and mass transfer problems, even in simple pipe flows [16]. For non-buoyant flows, measurements [19,20] have shown that turbulent heat flux in the flow direction is two or three times larger than that normal to the wall, even though the streamwise temperature gradient is much smaller than its normal counterpart. For buoyant and/or compressible flows, the eddy diffusivity assumption is even less appropriate. Experimental measurements [21,22] in a vertical heated pipe flow showed a substantial change in the turbulence structure, thus implying a reversal of the direction of the axial turbulent heat flux (i.e., the axial heat flux was measured upward instead of downward as implied by the eddy diffusivity concept). It is because of the above-mentioned reasons that many recent contributions to turbulence modelling are devoted to developing low-Reynolds-number near-wall turbulence closures [9,10,14,23]. Although much progress has been achieved in recent years in the modelling of the Reynolds-stress transport equations [23], the modelling of the scalar field, on the other hand, is still rather primitive. The reason is that turbulent stresses are a very important input to the heat-flux equations. Therefore, model development of the latter depends largely on the availability and correctness of the Reynolds-stress model. Furthermore, heat-flux transport is influenced by more than one time scale [24]. Consequently, it is more difficult to achieve closure of the heat-flux transport equations than the Reynolds-stress equations. Besides, a shortage of reliable and relatively accurate near-wall heat-flux measurements also contributes to the slow development of a near-wall turbulence model for the heat fluxes. Comprehensive reviews of the modelling of turbulent heat transfer can be found in Refs. 16 and 25.

Due to the difficulties mentioned above, the most common approach to turbulent heat transfer studies is to model the normal heat flux using the classical Boussinesq approximation.

3

The unknown eddy diffusivity for heat is calculated by prescribing a turbulent Prandtl number, Pr_t. Realizing the limitation of the calculation methods based on prescribed Pr_t, researchers try to improve the modelling by resorting to two-equation [26] and algebraic-flux models [27] for heat transport. Despite some successes, it is still believed that the most reliable prediction methods are those based on a second-moment closure. The reason is that the turbulent interactions which generate the Reynolds stresses and heat fluxes can be treated with less empiricism. Moreover, for those processes which cannot be so handled, a more rational and systematic set of approximations can be derived.

A first attempt to compute turbulent heat transfer process using high-Reynolds-number second-moment closures was made by meteorological fluid dynamicists [28,29,30]. On the other hand, applications of similar second-moment turbulence closures to engineering heat transfer problems have been attempted by Baughn et al. [31] and Launder and Samaraweera [32], among others. Recently, the model was extended by Yoo and So [15] to calculate isothermal, variable-density flows in a sudden-expansion pipe. In their approach, the flow and turbulence field were resolved by a low-Reynolds-number second-moment closure. The scalar flux equation was closed by high-Reynolds-number models and the near-wall scalar fluxes were evaluated assuming a constant turbulent Schmidt number. This is one way to handle the scalar flux transport equations for the near-wall flow, even though the approach is known to be quite inappropriate for most turbulent heat and mass transfer problems of engineering interests [15,16,17]. The reason for this appears to be that, so far, no suitable near-wall second-moment closure for scalar flux transport has been developed. This is due, in part, to a lack of detailed near-wall scalar flux measurements and, partially, to the unavailability of an asymptotically correct near-wall Reynolds-stress model.

Recently, Lai and So [23] have developed a near-wall Reynolds-stress turbulence model that can correctly predict the anisotropy of the turbulent normal stresses. The success of that model provides the impetus to extend the approach of Ref. 23 to model turbulent heat transport near a wall. It is noted, however, that the modelling of the dissipation rate of temperature variance is quite

4

immature, even the high-Reynolds-number version of the modelled equation is not well developed. In view of this, Lai and So [33] concentrated their effort on the modelling of near-wall heat-flux transport assuming temperature to be a passive scalar in the flow. Therefore, their near-wall heat-flux model is equally valid for mass transport where mass is also a passive scalar. Their approach is similar to that outlined in Ref. 23 and is based on the limiting wall behavior of the heat-flux transport equations. This way, the modelled equation is valid all the way to the wall and the assumptions of a temperature wall function and a constant turbulent Prandtl number are not required. Their model is validated against fully-developed pipe flow data with uniform heat flux prescribed at the wall [19,20,34,35]. The result is very encouraging.

3. Objectives

With the availability of a near-wall Reynolds-stress and heat-flux model, the time is now ripe for its extension to flows where temperature cannot be considered as a passive scalar, such as in a compressible flow. This means that the transport equations for the temperature variance and its dissipation rate have to be solved simultaneously with the governing mean flow and energy equations, the Reynolds-stress equations and the heat-flux equations in a second-moment closure of the problem. Therefore, near-wall models for the equations governing the transport of the temperature variance and its dissipation rate are also required, in addition to the near-wall model for Reynolds stresses and heat fluxes. The present project attempts to accomplish these objectives using the approach outlined by Lai and So [23,33] in their modelling of incompressible near-wall Reynolds stresses and heat fluxes. More specifically, the present objectives can be stated as follows.

(1)   To extend the near-wall Reynolds-stress and heat-flux model of Lai and So [23, 33] to compressible flows.

(2)   To formulate a near-wall closure for the temperature variance transport equation.

5

(3)   To formulate a near-wall closure for the equation that governs the transport of the dissipation rate of the temperature variance.

(4)   To validate these closures using data from heat and mass transfer experiments.

(5)   To extend these closures to compressible flows and to validate them against high speed flow data.

4.   Progress to-date

Since the beginning of this contract period, work on extending the incompressible near-wall Reynolds-stress models of Lai and So [23] has been carried out. An oral presentation of this work has been made at NASA Langley Research Centre on February 22. Various suggestions were given on how to further improve the near-wall models; in particular, the modelling of the compressible dissipation function. The splitting of this function into a solenoidal part and a compressible part was suggested. This way, the solenoidal part is not affected by compressibility effects and could be modelled by directly extending the incompressible near-wall models for the dissipation function to compressible flows. A second suggestion concerned with the incorrect near-wall behavior of ε, the dissipation rate of the turbulent kinetic energy. Essentially all existing modelled ε-equations give this incorrect behavior. The suggestion is to formulate a new ε-equation so that the correct near-wall behavior of ε according to direct simulation data could be reproduced.

Work on these two suggestions has been carried out. The suggested split of the dissipation function has been adopted and a near-wall model for the solenoidal part has been formulated. This work will be reported in the next progress report when the formulation on the heat-flux model is discussed. The present report deals with work carried out to improve the ε-equation. In the following, a summary report is given on the near-wall modelling and validation of the ε-equation.

5. Near-wall modelling and validation of the dissipation-rate equation

According to the near-wall Reynolds-stress closure of Lai and So [23], the models for the dissipation and velocity pressure-gradient correlation terms are required to satisfy the asymptotic near-wall behavior of the exact terms in the Reynolds-stress equation. Good predictions of low-Reynolds-number plane channel flows [36,37] are obtained. The only exception is the near-wall distribution of ε. Direct simulation data shows that ε reaches a plateau in the near-wall region before increases to a maximum at the wall. The prediction, on the other hand, gives a maximum away from the wall and a wall value that is about half that of the direct simulation result. When the closure is applied to calculate a curved channel flow [38], the same behavior is obtained. In spite of the discrepancy noted in the prediction of ε, the near-wall behaviors of all other turbulence properties are calculated correctly, including the wall friction velocities on the convex and concave side of the channel [39]. These results seem to suggest that a correct prediction of ε near a wall is not so important as far as the other turbulence properties are concerned. Further evidence in support of this conclusion can be gleaned from the heat transfer modelling calculations [33].

The reason for this discrepancy could be traced to the modelled ε-equation. The complicated exact ε-equation is modelled to give

$$C_\varepsilon = D_\varepsilon^\nu + D_\varepsilon^T + P_\varepsilon - D_\varepsilon + \xi \tag{1}$$

where the terms from left to right represent convection, viscous diffusion, turbulent diffusion, mean-shear production and viscous dissipation of ε, and ξ is a near-wall correction for D_ε. Various arguments [14,40,41] have been used to justify the inclusion of ξ in Eq. (1) and different approaches have been proposed for the determination of ξ. Most approaches rely on a first-order near-wall balance of the ε-equation [40,41]. However, Shima [14] proposes to consider the coincidence condition,

$$\frac{\partial \epsilon}{\partial t} = \frac{\partial}{\partial t}\left(\nu\frac{\partial^2 k}{\partial x_j \partial x_j}\right) \quad , \tag{2}$$

which is guaranteed by the exact equation but not necessarily by the modelled equation. In Eq. (2), k is the turbulent kinetic energy, ν is fluid kinematic viscosity, x_j is the jth component of the spatial coordinate and t is time. The near-wall Reynolds-stress closure [23,33,39] adopts this idea to derive ξ. Even then, the predicted ϵ behavior near a wall is incorrect.

According to Mansour et al. [42], this incorrect behavior could be traced to the models proposed for P_ϵ and D_ϵ. Their analysis shows that existing models for P_ϵ and D_ϵ, such as $P_\epsilon = C_{\epsilon 1}(\epsilon/k)P$ and $D_\epsilon = C_{\epsilon 2}(\epsilon\tilde{\epsilon}/k)$ under-predict P_ϵ and D_ϵ in the region $0 \leq y^+ < 15$. Here, $C_{\epsilon 1}$ and $C_{\epsilon 2}$ are model constants, P is the production of k, $\tilde{\epsilon} = \epsilon - 2\nu(\partial\sqrt{k}/\partial x_j)^2$, $y^+ = yu_\tau/\nu$, u_τ is the friction velocity and y is the normal coordinate measured from the wall. As a result, they suggest modifying P_ϵ and D_ϵ by multiplying them by f_1 and f_2, respectivley. These are damping functions whose values quickly approach one for large y^+. They use the direct simulation data to determine f_1 and f_2 and then apply the numerically determined f_1 and f_2 to P_ϵ and D_ϵ. The resultant k-ϵ closure calculations give excellent agreement with the direct simulation data. They also point out the importance of modelling $-\overline{uv}$, the turbulent shear stress. In general, $-\overline{uv}$ is given by

$$-\overline{uv} = \nu_t(\partial U/\partial y) = C_\mu f_\mu (k^2/\epsilon)\,(\partial U/\partial y), \tag{3}$$

for simple wall shear flow, where U is the mean flow velocity, f_μ is a damping function and C_μ is a model constant. The analysis of Mansour et al. [42] shows that the behavior of f_μ near a wall has a significant effect on the overall calculated k and ϵ.

Recently, Myong and Kasagi [43] suggest that if f_μ is modelled to give a near-wall behavior of y^{-1} as compared to a conventional behavior of y [40,41], then, only D_ϵ needs to be damped. In other words, f_1 can be set equal to one and they propose a new f_2 based on a form first put forward by Hanjalic and Launder [12]. Their k-ϵ closure calculations are in good

8

agreement with measurements. However, their calculated ε behavior near a wall is no different from those given in [14,23,33,29-41] and is contrary to that shown in [42]. A variety of other two-equation closures has been analysed by Speziale et al. [44]. Again, their calcualted ε behavior for a boundary-layer flow is contrary to that given in [45] and is similar to those obtained in [14,23,33,39-41,43]. Their results are calculated based on f_μ that behaves like y^{-1} near a wall. With the exception of ε, all other turbulence properties are predicted correctly compared to the data collected in [41]. Once again, their results tend to show that the problem of an incorrect near-wall behavior of ε is associated with the equation for the turbulent time scale.

The work in this period concentrates on making use of all these findings to seek modifications to P_ε and D_ε so that the resultant ε distribution mimicks the direct simulation results [36-38,45] in the near-wall region. Since the same ε-equation is used for both k-ε and Reynolds-stress closures, it is prudent to start with the k-ε closure. Certain constraints are imposed and these are the correct behavior of f_μ in the near-wall region and the accurate predictions of all turbulence properties and their limiting behavior near a wall. Furthermore, an asymptotic approach of the k-ε closure to its high-Reynolds-number version far away from a wall is also stipulated. In the process, it is hoped that the extent of the influence of the near-wall modifications on the whole flow could be assessed.

5.1   Modelling of the dissipation-rate equation

The k-ε closure to be investigated is given by the equations

$$\frac{Dk}{Dt} = \frac{\partial}{\partial x_j}\left(\nu\frac{\partial k}{\partial x_j}\right) + \frac{\partial}{\partial x_j}\left(\frac{\nu_t}{\sigma_k}\frac{\partial k}{\partial x_j}\right) + \widetilde{P} - \varepsilon \quad , \tag{4}$$

$$\frac{D\varepsilon}{Dt} = \frac{\partial}{\partial x_j}\left(\nu\frac{\partial \varepsilon}{\partial x_j}\right) + \frac{\partial}{\partial x_j}\left(\frac{\nu_t}{\sigma_\varepsilon}\frac{\partial \varepsilon}{\partial x_j}\right) + C_{\varepsilon 1}\frac{\varepsilon}{k}\widetilde{P} - C_{\varepsilon 2}f_\varepsilon\frac{\varepsilon^2}{k} \quad , \tag{5}$$

where σ_k, σ_ε, $C_{\varepsilon 1}$ and C_ε are model constants, $\widetilde{P} = \overline{u_i u_j}\,(\partial U_i/\partial x_j)$ and f_ε is a damping function to be determined. The wall boundary conditions for k and ε are given by $k_w = 0$ and $\varepsilon_w =$

9

$2\nu\left(\partial\sqrt{k}/\partial x_j\right)^2_w$. Here, the subscript w is used to denote the condition at the wall. On the other hand, the external boundary conditions depend on the type of flows considered. For boundary-layer flows, the conditions $k_\infty = 0$ and $\varepsilon_\infty = 0$ are appropriate, where subscript ∞ is used to denote the edge of the boundary layer. For internal flows, where a symmetry axis exists, the conditions $\partial k/\partial n = 0$ and $\partial \varepsilon/\partial n = 0$ can be specified. Here, n is a coordinate normal to the symmetry axis. In the present investigations, only stationary, two-dimensional thin shear layers or fully-developed turbulent flows are considered. Therefore, only the gradient normal to the flow direction is important and the turbulent shear stress is given by $-\overline{uv}$ alone. Thus simplified, the k and ε equations become

$$U\frac{\partial k}{\partial x} + V\frac{\partial k}{\partial y} = \frac{\partial}{\partial y}\left(\nu\frac{\partial k}{\partial y}\right) + \frac{\partial}{\partial y}\left(\frac{\nu_t}{\sigma_k}\frac{\partial k}{\partial y}\right) - \overline{uv}\frac{\partial U}{\partial y} - \varepsilon \quad , \tag{6}$$

$$U\frac{\partial \varepsilon}{\partial x} + V\frac{\partial \varepsilon}{\partial y} = \frac{\partial}{\partial y}\left(\nu\frac{\partial \varepsilon}{\partial y}\right) + \frac{\partial}{\partial y}\left(\frac{\nu_t}{\sigma_\varepsilon}\frac{\partial \varepsilon}{\partial y}\right) - C_{\varepsilon 1}\frac{\varepsilon}{k}\overline{uv}\frac{\partial U}{\partial y} - C_{\varepsilon 2}f_\varepsilon\frac{\varepsilon^2}{k} \quad , \tag{7}$$

where U and V are the mean velocities along x and y, respectively, and ν_t is given by $C_\mu f_\mu k^2/\varepsilon$.

The ε-equation could be improved by first considering the k-ε closures of Lai and So [23] and Myong and Kasagi [43] to investigate the source of the incorrect behavior of ε near a wall. The values of the model constants and the functions f_μ and f_ε for these two closures are summarized in Table 1. Since the original Lai and So [23] closure gives a ν_t that does not behave like y^3 near a wall, the f_μ used by Lai and So [23] has to be modified. The resultant f_μ is listed in Table 1 and the behavior of ν_t is found to be y^3 near a wall [36,43]. As a result, their f_ε funtion has to be modified to reflect the change in f_μ. In Table 1, f_ε for the Lai and So [23] closure is defined by combining their ξ and D_ε terms together to give $C_{\varepsilon 2}f_\varepsilon \varepsilon^2/k$. The function $f_{w,2}$ is given by $f_{w,2} = e^{-(R_t/64)^2}$ and $R_t = k^2/\nu\varepsilon$ is the turbulent Reynolds number.

In order to understand the incorrect near-wall behavior of ε given by these two closures, they are used to calculate the flat plate boundary layer data collected in [41,47]. The results shown

in Figs. 1-3 are for a distance of $x \cong 5$ m, $R_x = 1.156 \times 10^7$ and $R_\theta = 16,465$, where R_x and R_θ are the Reynolds number based on x and momentum thickness θ, respectively. Figure 1 gives the result of the mean flow while Figs. 2 and 3 give the distributions of k and ϵ near the wall. The plots are given in terms of y^+, u^+, k^+ and ϵ^+ where $u^+ = U/u_\tau$, $k^+ = k/u_\tau^2$ and $\epsilon+ = \epsilon\nu/u_\tau^4$. It can be seen that the predictions of both closures are essentially identical and are in good agreement with the data of [41] and the predictions of [44]. However, the near-wall behavior of ϵ^+ is incorrect compared to the data of [36,45,46].

Table 1 Constants and model functions for the three k-ϵ closures considered.

Source	C_μ	$C_{\epsilon 1}$	$C_{\epsilon 2}$	σ_k	σ_ϵ	f_μ	f_ϵ	ϵ_w
Myong & Kasagi [43]	0.09	1.4	1.8	1.4	1.3	$(1 + 3.45 / \sqrt{R_t})$ $\times (1 - e^{-y^+/70})$	$\left[1 - \frac{2}{9}e^{-(R_t/6)^2}\right]$ $\times \left(1 - e^{-y^+/5}\right)^2$	$\nu\dfrac{\partial^2 k}{\partial y^2}$
Lai & So [23]	0.092	1.4	1.72	1.0	1.4	$(1 + 3.45 / \sqrt{R_t})$ $\times \tanh(y^+/95)$	$\dfrac{\tilde{\epsilon}}{\epsilon}\left[1 - \dfrac{C_{\epsilon 2} - 2}{C_{\epsilon 2}}f_{w,2} - \dfrac{3}{2}\dfrac{f_{w,2}}{C_{\epsilon 2}}\left(\epsilon^{*2}/\epsilon\tilde{\epsilon}\right)\right]$	$\nu\left(\dfrac{\partial\sqrt{k}}{\partial y}\right)^2$
Present	0.096	1.48	1.78	1.01	1.45	$(1 + 3.45 / \sqrt{R_t})$ $\times \tanh(y^+/120)$	$\dfrac{\tilde{\epsilon}}{\epsilon}\left[1 + \dfrac{2f_{w,2}}{C_{\epsilon 2}} - \dfrac{3}{2}\dfrac{f_{w,2}}{C_{\epsilon 2}}\left(\epsilon^{*2}/\epsilon\tilde{\epsilon}\right)\right]$	$\nu\left(\dfrac{\partial\sqrt{k}}{\partial y}\right)^2$

According to Mansour et al. [42], a possible source of error for the incorrect ϵ behavior is the f_ϵ function. A plot of the f_ϵ behavior for these two closures is shown in Fig. 4. The results show that both closures give a f_ϵ that increases monotonically from zero at the wall to one around $y^+ = 30$. Near the wall, the behavior of k^+ and ϵ^+ is given by [36,41,46]

$$k^+ = a_k\, y^{+2} + b_k\, y^{+3} + \ldots, \tag{8}$$

$$\epsilon^+ = 2a_k + 4b_k y^+ + \ldots \tag{9}$$

Therefore, f_ε should behave like y^{+2} very near a wall, otherwise, the term $C_{\varepsilon 2}f_\varepsilon\varepsilon^2/k$ would increase indefinitely as the wall is approached. This quadratic behavior is guaranteed by the f_ε functions listed in Table 1. However, the near-wall behavior of the modelled f_ε is not consistent with the simulation data of [36]. Mansour et al. [42] used that data to calculate f_ε. According to their calculation, f_ε increases steeply to overshoot one and then decreases to approach one asymptotically. The behavior is like the present f_ε curve shown in Fig. 4. This means that, if the predicted ε^+ is to mimic the simulation data of [36,45], a f_ε that overshoots one in the near-wall region has to be formulated. Furthermore, the proposed f_ε should behave like y^{+2} very near a wall and asymptote to one around $y^+ = 30$ in order to give results identical to those given by [23,43,44]. The closure should also give the correct limiting behavior for k^+/ε^+y^{+2}, $(-\overline{uv^+}/y^{+3})_w$ and ε_w^+, where $-\overline{uv^+} = -\overline{uv}/u_\tau^2$. According to the data of [36,46], ε_w^+ varies from 0.18 to 0.22 and $(-\overline{uv^+}/y^{+3})_w = 8.5 \times 10^{-4}$. On the other hand, k^+/ε^+y^{+2} is exactly 0.5 at the wall. These values, with the exception of k^+/ε^+y^{+2}, are listed in Table 2 for comparison.

An inspection of the f_ε functions of [23,43] plotted in Fig. 4 reveals that they could be modified and made to mimic the direct simulation behavior of [36,45]. This means that f_ε has to increase more rapidly and possibly overshoots one in the region $0 \leq y^+ < 20$. Such a behavior could be reproduced by modifying the f_ε function of [23] to that shown in Table 1.

5.2 Validation of the improved dissipation-rate equation

The improved f_ε is again used in Eq. (7) to calculate the flat plate boundary layer flow [41,47]. Calculations are carried out for the same R_x and R_θ and the new results are plotted in Figs. 1-4 for comparison with the previous results. Immediately, the following conclusions can be drawn from these comparisons. First and foremost, the mean U distribution is not affected by f_ε (Fig. 1). As a result, the U^+ versus ln y^+ plots for the three k-ε closures listed in Table 1 are identical and the log region can be described by

12

$$U^+ = \frac{1}{0.41} \ln y^+ + 4.7. \tag{10}$$

Secondly, the distributions of k^+ and ε^+ beyond $y^+ = 100$ are essentially the same; thus indicating that f_ε has little or no effect on the behavior of k^+ and ε^+ beyond $y^+ = 100$ (Figs. 2 and 3). Thirdly, f_ε significantly affects the behavior of ε^+ (Fig. 3) and much less so the behavior of k^+ (Fig. 2) in the region $0 \le y^+ < 20$. Fourthly, the value of ε_w^+ is very much affected by the rise of f_ε in the region $0 < y^+ < 10$; the more rapidly f_ε increases in the region $0 < y^+ < 10$, the higher the ε_w^+ value (Figs 3 and 4). Finally, the near-wall behavior of ε^+ is entirely controlled by f_ε. The improved f_ε gives a maximum ε^+ at the wall while the other two f_ε's give a maximum ε^+ away from the wall. Furthermore, the closures of Myong and Kasagi [43] and Lai and So [23] predict the location where the maximum ε^+ occurs to be at about $y^+ = 10$, which approximately coincides with the location of the second maximum of ε^+ in the present closure prediction (Fig. 3).

Table 2. Comparison of calculated wall properties with data

Source	$C_f \times 10^3$	a_k	$\left(\frac{-\overline{uv^+}}{y^{+3}}\right) \times 10^4$	$\varepsilon_w^+ = 2a_k$
Present	2.39	0.098	6.5	0.196
Speziole et al. [44]	2.45	0.047	-	0.094
Myong and Kasagi [43]	2.41	0.054	7.3	0.108
Chien [40]	2.44	0.056	-	0.113
Lai and So [23]	2.40	0.076	6.5	0.152
Kim et al. [36]	-	0.090	-	0.18
Nishino and Kasagi [46]	-	0.110	8.5	0.22
Patel et al. [41] and Weighardt and Tillmann [47]	2.43	0.025 to 0.050	-	0.05 to 0.10

13

The predicted near-wall ε^+ distributions are compared with the direct simulation data of [36,45] in Fig. 5. Spalart's data [45] is from a flat plate boundary layer at $R_\theta = 1410$ while the data of Kim et al. [36] is from a fully-developed plane channel flow at a $Re_D = 6600$. Here, Re_D is the Reynolds number based on channel width and centerline velocity. Since the Reynolds numbers of these flows are widely different from the present calculations, a quantitative comparison between the various results is not advisable. However, a qualitative comparison is appropriate. The present calculated ε^+ behavior near the wall is similar to that obtained from direct simulation. Furthermore, the y^+ region where the plateau of ε^+ occurs is correctly predicted to be around $5 < y^+ < 15$. On the other hand, the predicted wall value is between that obtained by Spalart [45] and Kim et al. [36]. The other closure predictions are contrary to the direct simulation results and give a totally incorrect trend in the near-wall region.

Very close to the wall, independent of the flow Reynolds number, the behavior of k^+, ε^+ and $-\overline{uv}^+$ is given by

$$k^+/y^{+2} = a_k + O(y^+), \tag{11}$$

$$k^+/\varepsilon^+ y^{+2} = 0.5 + O(y^+), \tag{12}$$

$$-\overline{uv}^+/y^{+3} = a_{uv} + O(y^+). \tag{13}$$

According to direct simulation data [36] and measurements [46], a_k varies from 0.09 to 0.11. In other words, ε_w^+ should vary from 0.18 to 0.22. Also, $a_{uv} = 8.5 \times 10^{-4}$ according to [46]. These values are listed in Table 2 together with the calculated values. The plots of Eqs. (11) - (13) are shown in Figs. 6-8, respectively.

It can be seen that the present calculated a_k agrees well with data [36,46] while the a_k's predicted by the other two closures do not. The linear relation given by Eq.(11) holds true in the region $0 \leq y^+ < 2$ (Fig. 6). According to Eq.(12), $k^+/\varepsilon^+ y^{+2} = 0.5$. This is recovered exactly by

14

the present closure but not by the other two closures tested. All three closures, however, show that the variation of k^+/ϵ^+ with y^{+2} is linear in the region $0 \leq y^+ < 2$ (Fig. 7). On the other hand, the distribution of $\overline{-uv}^+$ versus y^{+3} is only linear in the region $0 \leq y^+ < 1$ (Fig. 8) and a_{uv} thus dteremined is highest for the closure of [43] and about the same for the present closure and that of [23]. These values are listed in Table 2 for comparison with the data of [46]. The present prediction is low by about 25% and it seems that the predicted a_{uv} is not affected by f_ϵ. Instead, it is influenced by f_μ. The present closure and that of [23] use the same f_μ but different f_ϵ and they give essentially the same a_{uv}. Since f_μ has little or no effect on the near-wall behavior of ϵ^+, the prediction of a_{uv} could be improved by changing f_μ.

A final comparison is made with C_f, the skin friction coefficient. The predicted values are listed in Table 2 for comparison with the mean data collected from [41, 47]. In addition, the predictions of Speziale et al. [44] and Chien [40] are also listed for comparison. It can be seen that all calculated and measured values of C_f are within 2% of each other.

The budget of k in the near-wall region is shown in Fig. 9. In this plot, only the viscous and turbulent diffusion of k, the production of k and the dissipation of k are shown. Since the convection of k is not important in the near-wall region, it is not shown in Fig. 9. At the wall, viscous diffusion balances dissipation. This balance extends to about $y^+ = 2$. In the region, $2 \leq y^+ < 15$, all four terms are of equal importance. Beyond $y^+ = 15$, the turbulence is in local equilibrium, that is, production of k balances the dissipation of k. These results show that the equilibrium turbulence assumption is applicable up to $y^+ = 15$. This behavior is similar to the direct simulation results of [36,45].

Since f_ϵ involves the derivatives of k at the wall and away from the wall, its numerical evaluation is not necessary stable. Therefore, an attempt is made to curve fit f_ϵ by a quadratic function near the wall and by a finite series of Legendre polynomials beyond about $y^+ = 2$. These

two functions should combine to give a correct behavior of f_ε in the near-wall region. The final functions thus determined are given by

$$f_\varepsilon = Cy^{+2} \qquad 0 \leq y^+ \leq 2 \qquad\qquad (14a)$$

$$f_\varepsilon = \Sigma_{n=0}^{7} C_n P_n(y^+) \qquad 2 \leq y^+ < 11 \qquad\qquad (14b)$$

where P_n is the Legendre polynomial of order n and C = 0.0042438, C_0 = 0.755123, C_1 = 0.562578, C_2 = -0.438464, C_3 = -0.018244, C_4 = 0.242495, C_5 = -0.101070, C_6 = -0.064993 and C_7 = 0.057071. A plot of these functions and the original f_ε are shown in Fig. 10. It can be seen that the curve fit f_ε replicates the original curve very well. The new f_ε is used to repeat the calculation of the flat plate boundary layer. Essentially the same results are obtained. One advantage of this new f_ε is that the numerical difficulties associated with the evaluation of the derivatives of k at and near the wall have been avoided. As a result, the numerical calculation is a lot more stable than before.

6.   Conclusions

Based on this study, the following conclusions can be drawn.

(i)   It is not necessary to modify P_ε and propose a near-wall correction function ξ to bring the ε-equation to balance in the near-wall region.

(ii)   It is only necessary to modify the dissipation term by a damping function f_ε in the ε-equation.

(iii)   The near-wall behavior of ε is very much affected by f_ε while the flow properties beyond $y^+ = 50$ are not much influenced by f_ε and the near-wall behavior of ε.

(iv)   A f_ε has been found where the near-wall behavior of ε is reproduced correctly.

(v)   The limiting values of k, ε and $-\overline{uv}$ are predicted correctly by the improved k-ε closure.

(vi)   Other k-ε closures examined also give correct predictions of the flow properties beyond y^+ = 50. However, in the region, $0 \le y^+ < 50$, the predictions are at variance with the present closure calculations.

(vii)   The new f_ε is numerically stable near the wall.

7.   Plans for next period

The plans for the next period are:

(i)   To further validate the ε-equation, such as applying it to calculate internal and complex flows.

(ii)   To extend and implement the ε-equation to compressible flows.

(iii)   To complete the extension of the incompressible near-wall heat-flux models to compressible flows.

References

1.   Wilcox, D.C. and Alber, I.E., "A turbulence model for high speed flows," Proc. of the 1972 Heat Transfer and Fluid Mechanics Institute, Stanford University Press, 231-252, 1972.

2.   Bradshaw, P., "Compressible turbulent shear layers," Ann. Rev. Fluid Mech. 9, 33-64, 1977.

3.   Rubesin, M.W., "A one-equation model of turbulence for use with the compressible Navier-Stokes equations," NASA TM-X-73-128, 1976.

4.   Viegas, J.R., and Horstman, C.C., "Comparison of multiequation on turbulence models for several shock boundary layer interaction flows," AIAA Journal 17, 811-820, 1979.

5.   Vandromme, D., Ha Minh, H., Viegas, J.R., Rubesin, M.W. and Kollman, W., "Second order closrue for the calculation of compressible wall bounded flows with an implicit Navier-Stokes solver," 4th Turbulent Shear Flows Conferences, Karlsruhe, 1983.

6.   Morkovin, M., "Effects of compressibility on turbulent flows," Mecanique de la turbulence, C.N.R.S., edited by A.Favre, 367-380, 1962.

7. Bradshaw, P., "The effect of mean compression or dilatation on the turbulence structure of supersonic boundary layers," J. Fluid Mech. **63**, 449-458,1974.

8. Oh, Y.H., "Analysis of two-dimensional free turbulent mixing," AIAA Paper No. 74594, 1974.

9. Rodi, W., "Recent developments in turbulence modelling," Proc. 3rd Int. Symp. on Refined Flow Modelling and Turbulence Measurements, Tokyo, July 26-28, 1988.

10. Launder, B.E. and Tselepidakis, D.P., "Contribution to the second-moment modelling of sublayer turbulent transport," Proc. Zaric Memorial International Seminar on Wall Turbulence, Dubrovnik, Yugoslavia, 1988.

11. Cousteix, J., "Three-dimensional and unsteady boundary layer computation," Ann. Rev. Fluid Mech. **18**, 173-196, 1986.

12. Hanjalic, K. and Launder, B.E., "Contribution towards a Reynolds-stress closure for low-Reynolds-number turbulence," J. Fluid Mech. **74**, 593-610, 1976.

13. So, R.M.C. and Yoo, G.J., "Low-Reynolds-number modelling of turbulent flows with and without wall transpiration," AIAA Journal **25**, 1556-1564, 1987.

14. Shima, N., "A Reynolds-stress model for near-wall and low-Reynolds-number regions," J. Fluids Eng. **110**, 38-44, 1988.

15. Yoo, G.J. and So, R.M.C., "Variable density effects on axisymmetric sudden-expansion flows," Int. J. Heat Mass Transfer **32**, 105-120, 1989.

16. Launder, B.E., "On the computation of convective heat transfer in complex turbulent flows," J. Heat Transfer **110**, 1112-1128, 1988.

17. Launder, B.E., "Numerical computation of convective heat transfer in complex turbulent flows: time to abandon wall functions?" Int. J. Heat Mass Transfer **27**, 1485-1491, 1984.

18. So, R.M.C., Lai, Y.G., Hwang, B.C., and Yoo, G.J., "Low-Reynolds-number modelling of flows over a backward-facing step," ZAMP **39**, 13-27, 1988.

19. Bremhorst, K. and Bullock, K.J., "Spectral measurements of temperature and longitudinal velocity fluctuations in fully developed pipe flow," Int. J. Heat Mass Transfer **13**, 1313-1329, 1970.

20. Bremhorst, K. and Bullock, K.J., "Spectral measurement of turbulent heat and momentum transfer in fully developed pipe flow," Int. J. Heat Mass Transfer **16**, 2141-2154, 1973.

21. Carr, A.D., Connor, M.A. and Buhr, H.O., "Velocity, temperature and turbulence measurements in air for pipe flow with combined free and forced convection," J. Heat Transfer **95**, 445-452, 1973.

22. Hochriter, L.E. and Sesonske, A., "Turbulent structure of isothermal and non-isothermal liquid metal pipe flow," Int. J. Heat Mass Transfer **17**, 113-128, 1974.

23. Lai, Y.G. and So, R.M.C., "On near-wall turbulent flow modelling," J. Fluid Mech., to appear, 1990.

24. Shih, T.H. and Lumley, J.L., "Influence of time scale ratio on scalar flux relaxation: modelling Sirivat and Warhaft's homogeneous passive scalar fluctuations," J. Fluid Mech. 162, 211-222, 1986.

25. Launder, B.E., "Heat and mass transport," in Turbulence - Topics in Applied Physics, 12, edited by P.Bradshaw, Springer, Berlin, 232-287, 1976.

26. Nagano, Y. and Kim, C., "A two-equation model for heat transport in wall turbulent shear flows," J. Heat Transfer 110, 583-589, 1988.

27. Prud'homme, M. and Elghobashi, S., "Turbulent heat transfer near the reattachment of flow downstream of a sudden pipe expansion," Numer. Heat Transfer 10, 349-368, 1986.

28. Monin, A.S., "On the symmetry of turbulence in the surface layer of air," IZV Atm. and Oceanic Phys. 1, 45-54, 1965.

29. Donaldson, C.duP., "Calculation of turbulent shear flows for atmospheric and vortex motions," AIAA Journal 10, 4-12, 1971.

30. Zeman, O. and Lumley, J.L., "Buoyancy effects in entraining turbulent boundary layers," Turbulent Shear Flows - I, Springer, Heidelberg, 295-306, 1979.

31. Baughn, J.W., Hoffman, M.A., Launder, B.E. and Samaraweera,D.S.A., "Three-dimensional turbulent heat transport in pipe flow: Experiment and model validation," ASME Paper No. 78-WA-HT-15, 1978.

32. Launder, B.E. and Samaraweera, D.S.A., "Application of a second-moment turbulence closure to heat and mass transport in thin shear flows - I. Two-dimensional transport," Int. J. Heat Mass Transfer 22, 1631-1643, 1979.

33. Lai, Y.G. and So, R.M.C., "Near-wall modelling of turbulent heat fluxes," Int. J. Heat Mass Transfer 33, 1429-1440, 1990.

34. Johnk, R.E. and Hanratty, T.J., "Temperature profiles for turbulent flow of air in a pipe - I. the fully developed heat transfer region," Chem. Engng. Sci. 17, 867-879, 1962.

35. Hishida, M., Nagano, Y. and Tagawa, M., "Transport processes of heat and momentum in the wall region of turbulent pipe flow," Proc. 8th International heat transfer conference, C.L.Tien et al., eds., Hemisphere, Washington, DC, Vol.3, 925-930, 1986.

36. Kim, J., Moin, P. and Moser, R., "Turbulence statistics in fully developed channel flow at low Reynolds number," J. Fluid Mech. 177, 133-166, 1987.

37. Mansour, N.N., Kim, J. and Moin, P., "Reynolds-stress and dissipation-rate budgets in a turbulent channel flow," J. Fluid Mech. 194, 15-44, 1988.

38. Moser, R.D. and Moin, P., "The effects of curvature in wall-bounded turbulent flows," J. Fluid Mech. 175, 479-510, 1987.

39. So, R.M.C., Lai, Y.G. and Hwang, B.C., "Near-wall turbulence closure for curved flows," AIAA Journal, to appear, 1991.

40. Chien, K.Y., "Predictions of channel and boundary-layer flows with a low-Reynolds-number two-equation model of turbulence," AIAA Journal 20, 33-38, 1982.

41. Patel, V.C., Rodi, W. and Scheuerer, G., "Turbulence models for near-wall and low-Reynolds-number flows," AIAA Journal 23, 1308-1319, 1985.

42. Mansour, N.N., Kim, J. and Moin, P., "Near-wall k-εturbulence modeling," AIAA Journal 27, 1068-1073, 1989.

43. Myong, H.K. and Kasagi, N., "A new approach to the improvement of k-ε turbulence model for wall bounded shear flows," JSME International Journal, Series II 33, 63-72, 1990.

44. Speziale, C.G., Abid, R. and Anderson, E.C., "A critical evaluation of two-equation models for near wall turbulence," AIAA Paper No. 90-1481, 1990.

45. Spalart, P.R., "Direct simulation of a turbulent boundary layer up to R_θ = 1410," J. Fluid Mech. 187, 61-98, 1988.

46. Nishino, K. and Kasagi, N., "Turbulence statistics measurement in a two-dimensional channel flow using a three-dimensional particle tracking velocimeter," Seventh Symp. on Turbulent Shear Flows, Stanford University, August 21-23, 22.1.1-22.1.6, 1989.

47. Wieghardt, K. and Tillmann, W., "On the turbulent friction layer for rising pressure," NACA TM-1314, 1951.
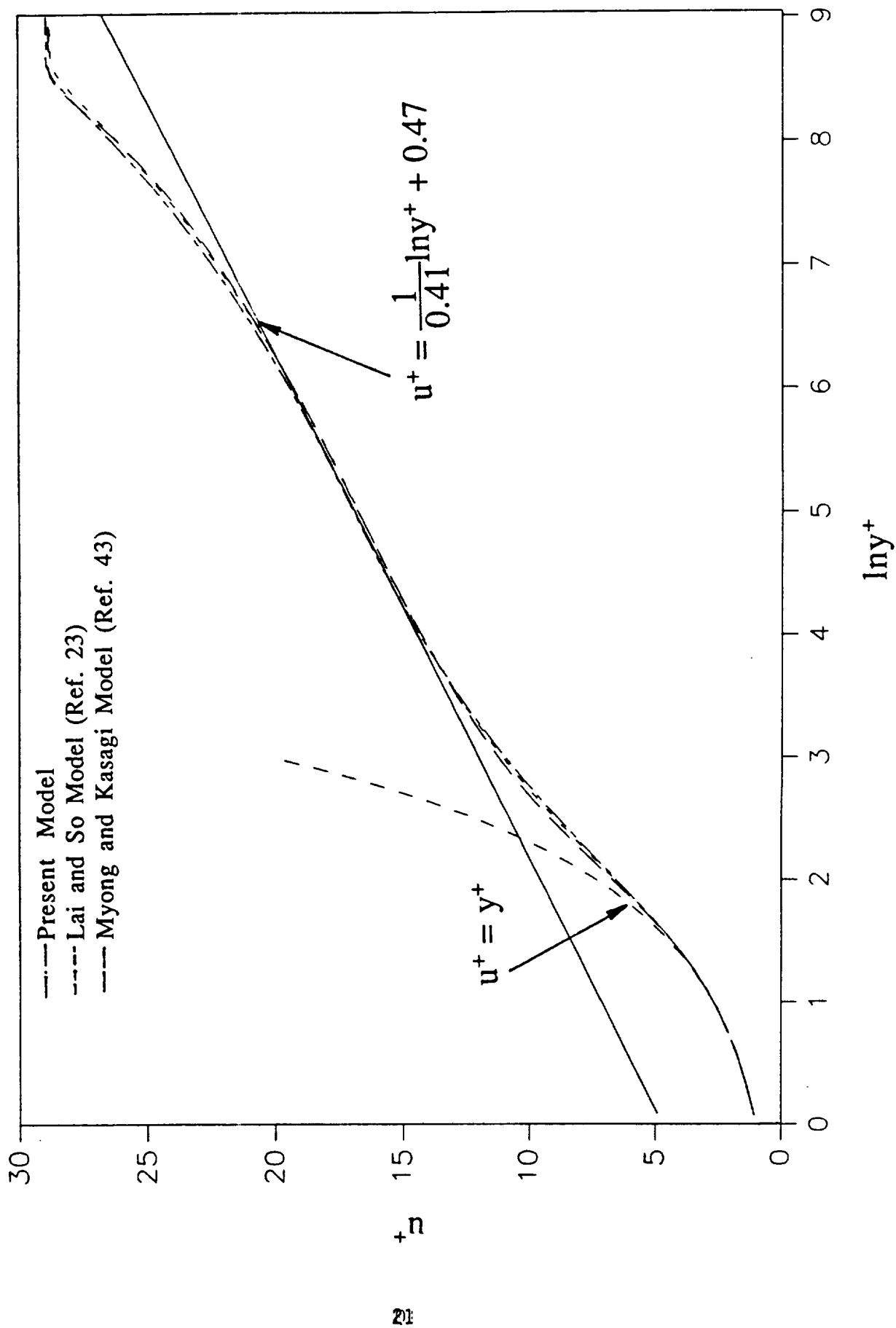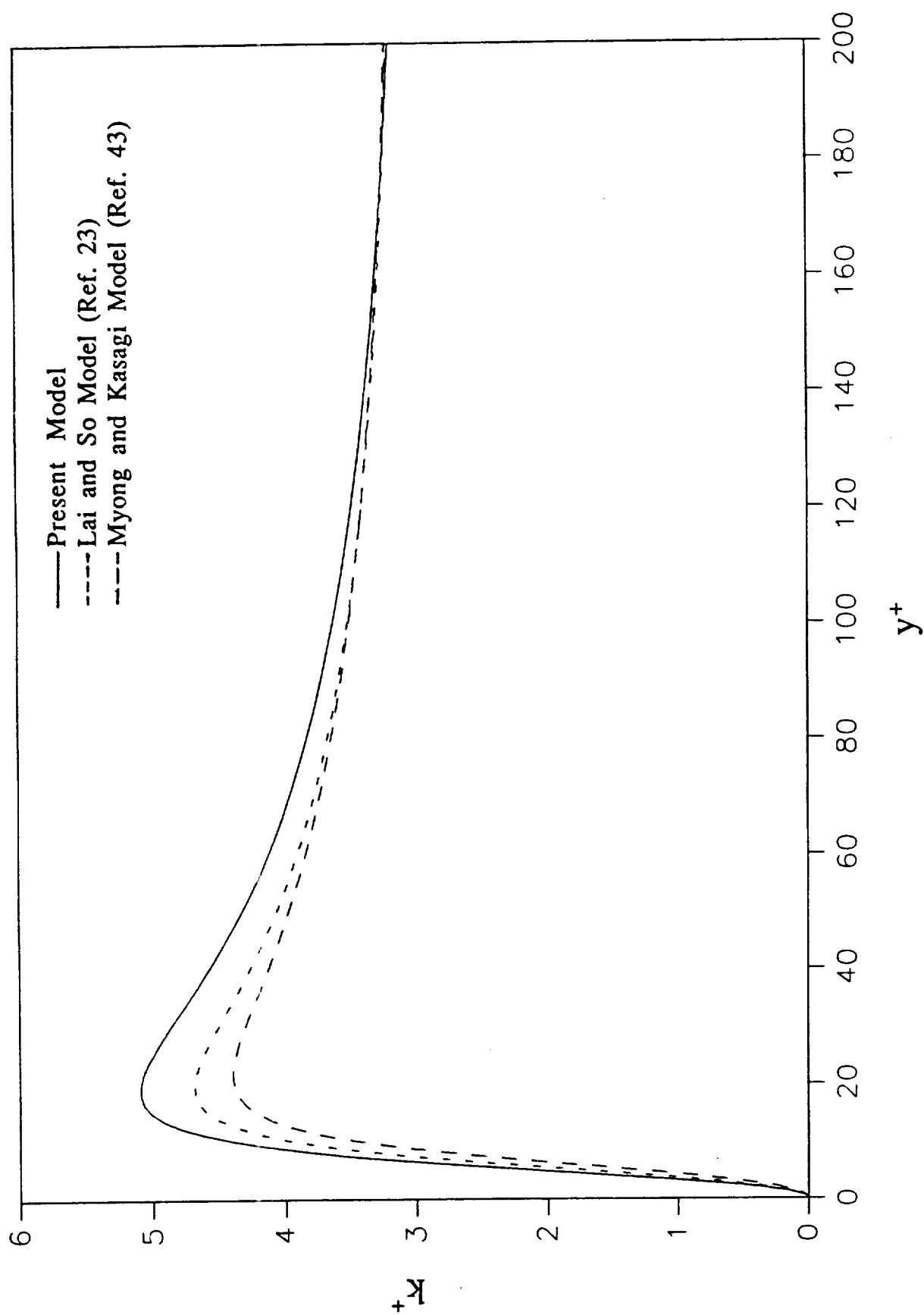
Figure 1 The calculated velocity in semi-log plot.

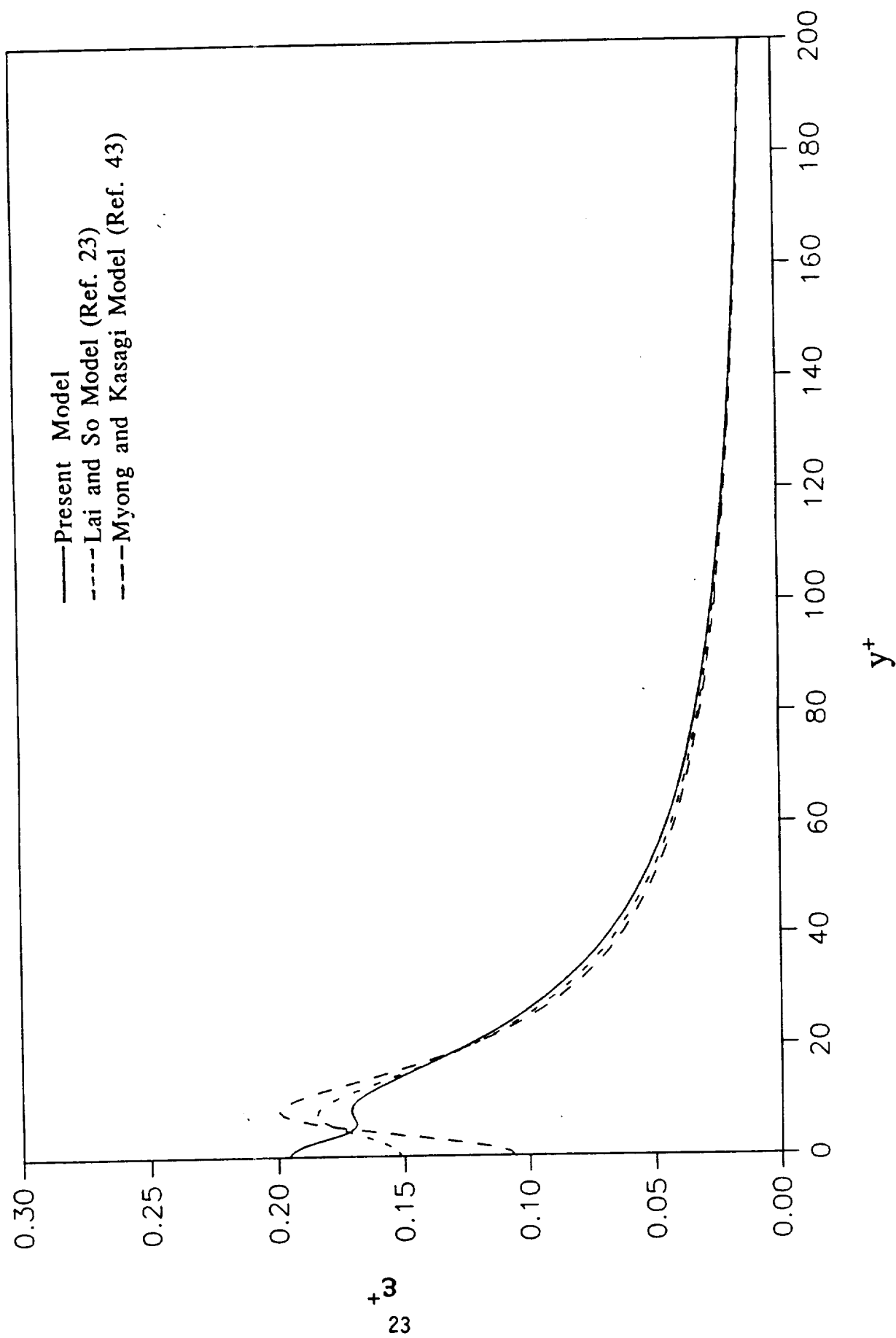Figure 2 Comparison of the calculated k in the near-wall region.

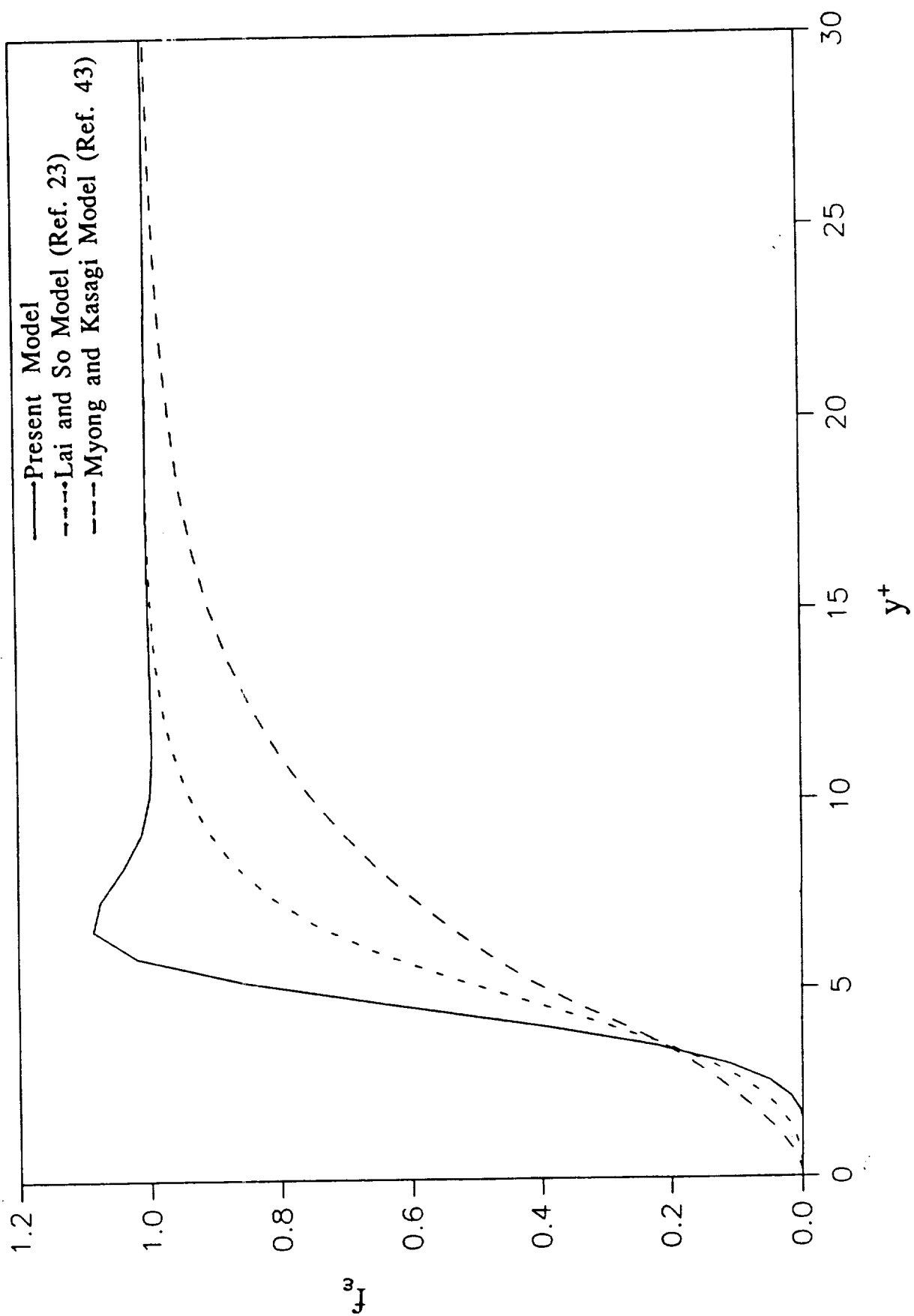Figure 3   Comparison of the calculated dissipation rate in the near-wall region.

23

Figure 4 Behavior of the dissipation damping function in the near-wall region.
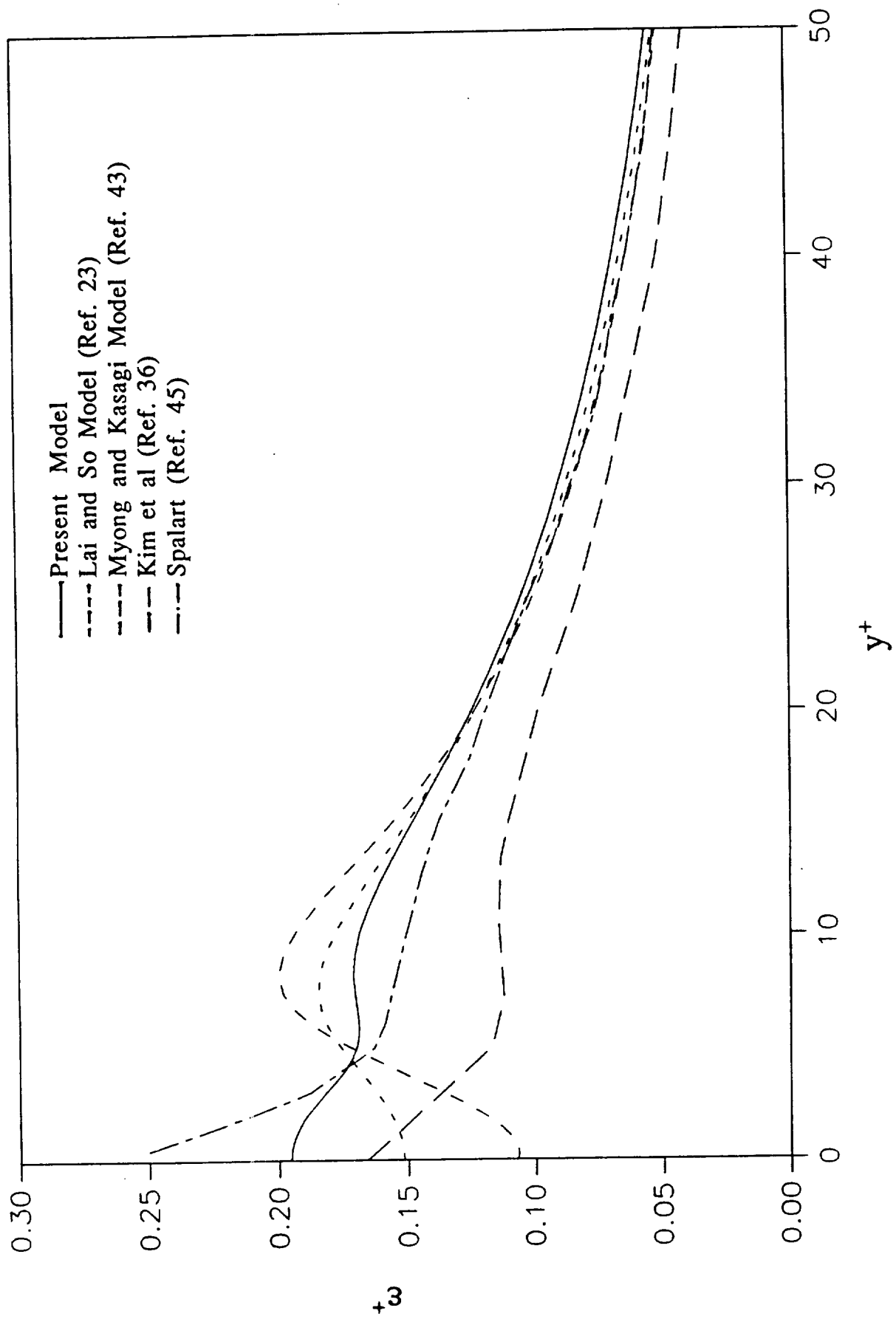
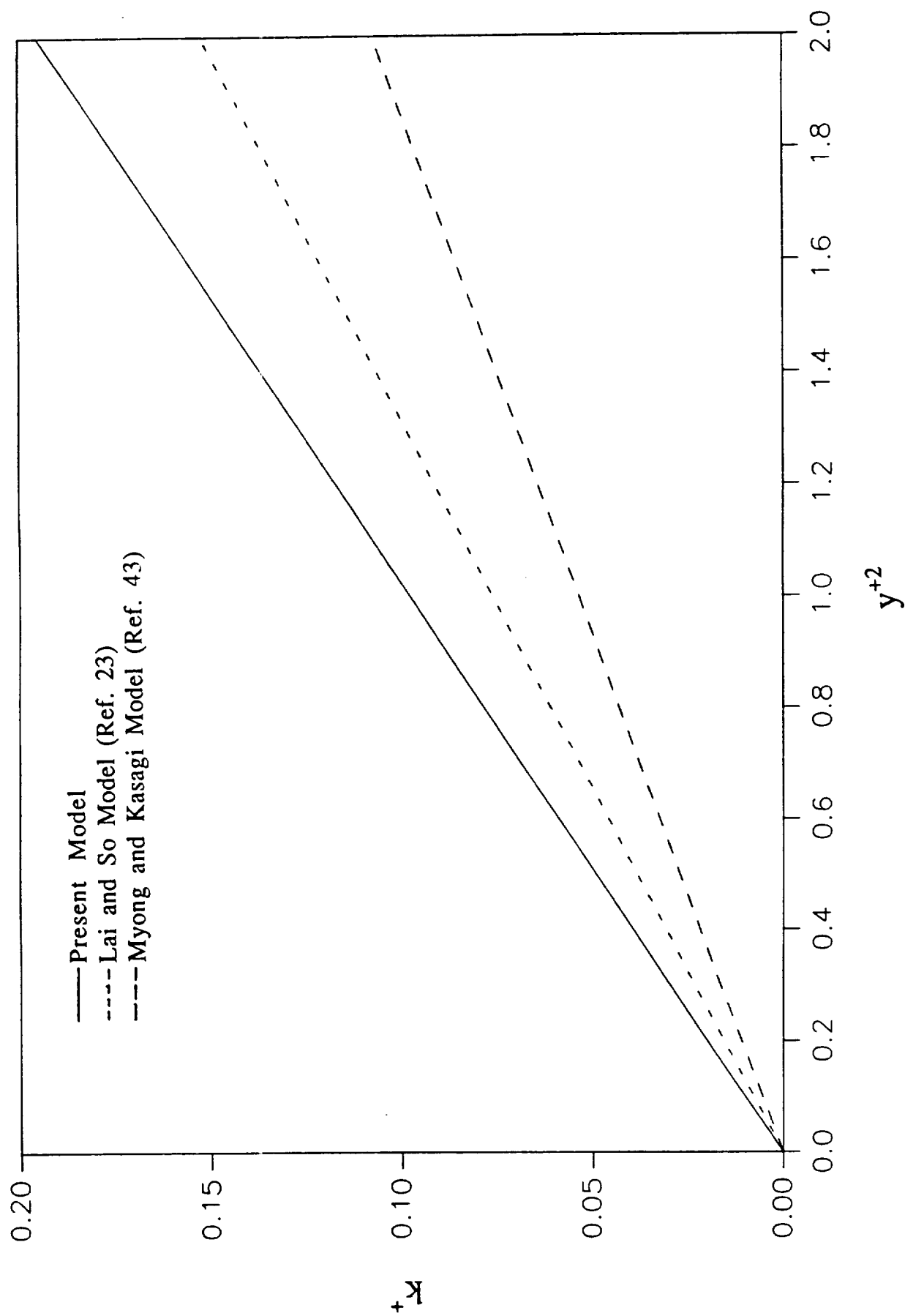Figure 5 Comparison of the dissipation rate with data in the near-wall region.

Legend:
- Present Model
- Lai and So Model (Ref. 23)
- Myong and Kasagi Model (Ref. 43)
- Kim et al (Ref. 36)
- Spalart (Ref. 45)

ε^+

y^+

25

Figure 6 The calculated slope of k at the wall.
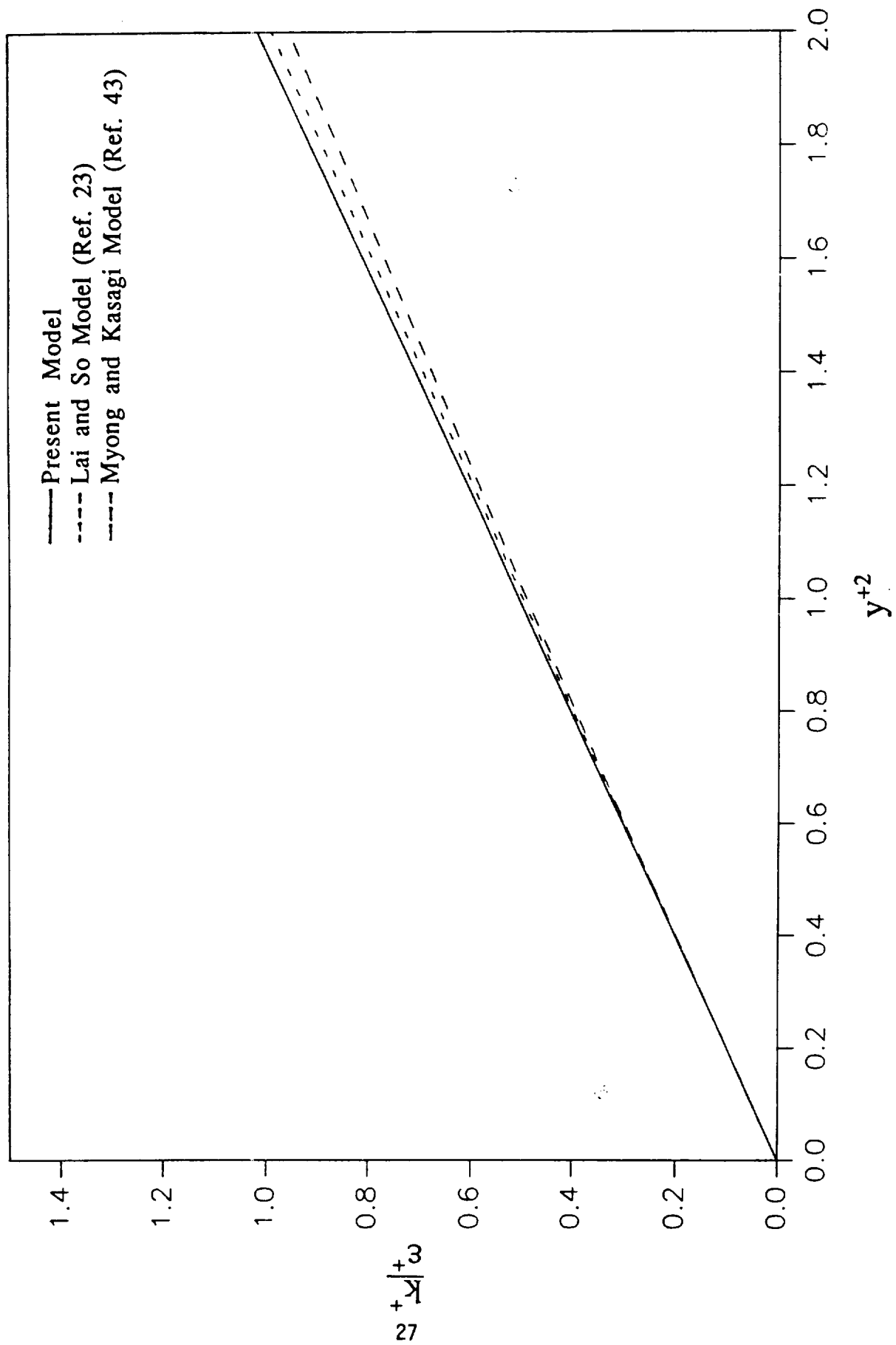
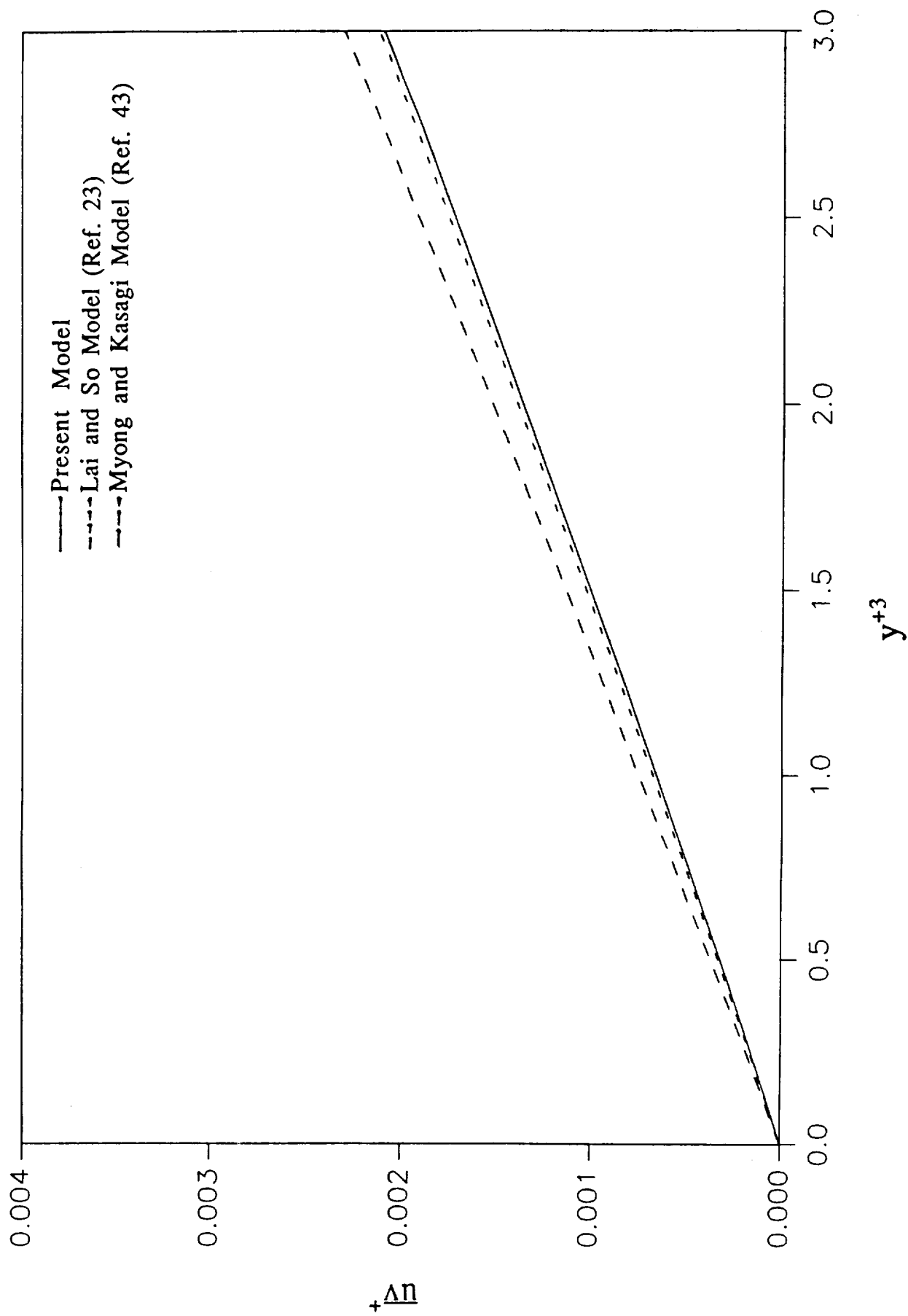Figure 7   The calculated slope of k over dissipation rate at the wall.

27

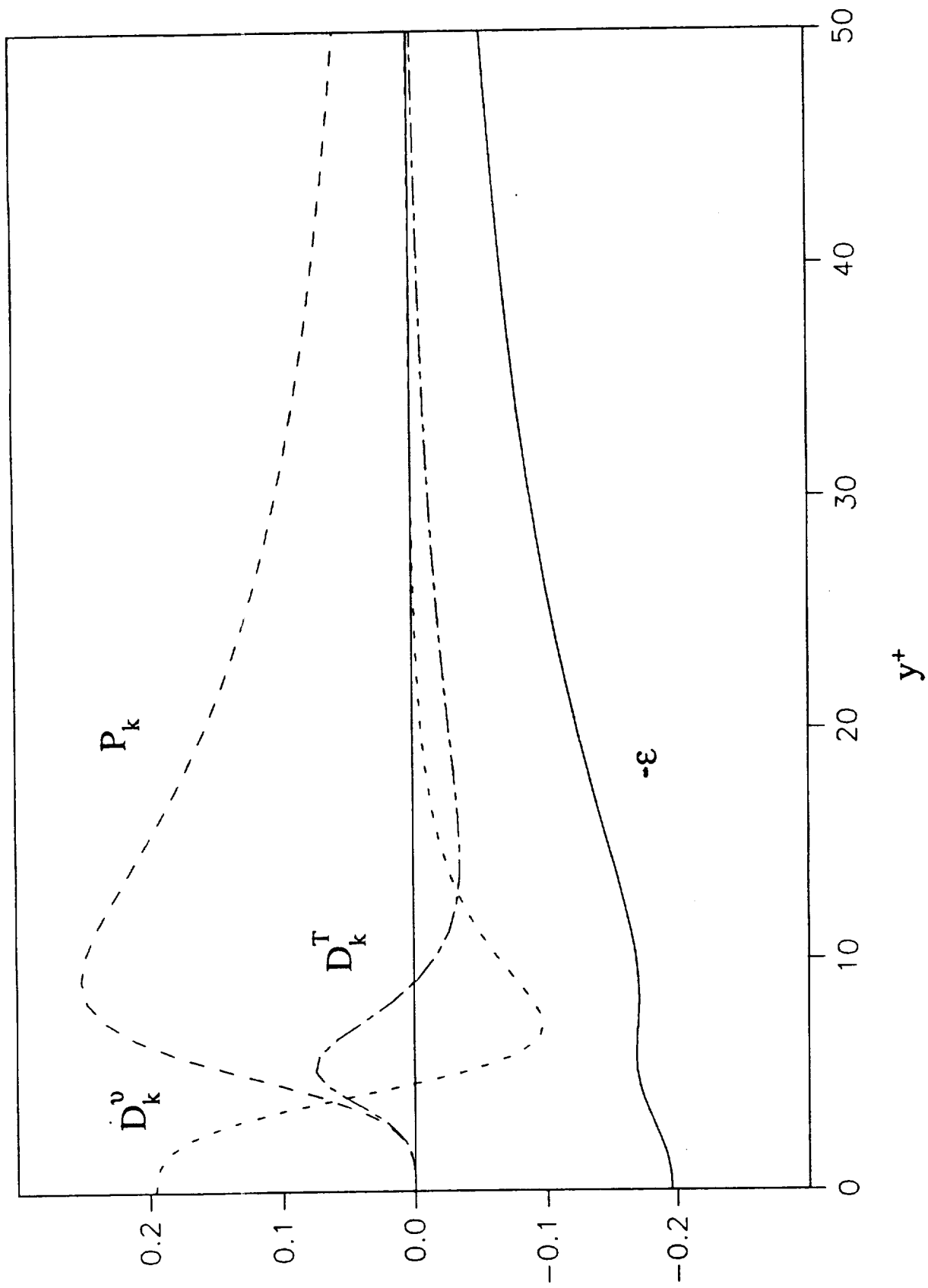Figure 8 The calculated slope of the turbulent shear stress at the wall.

28

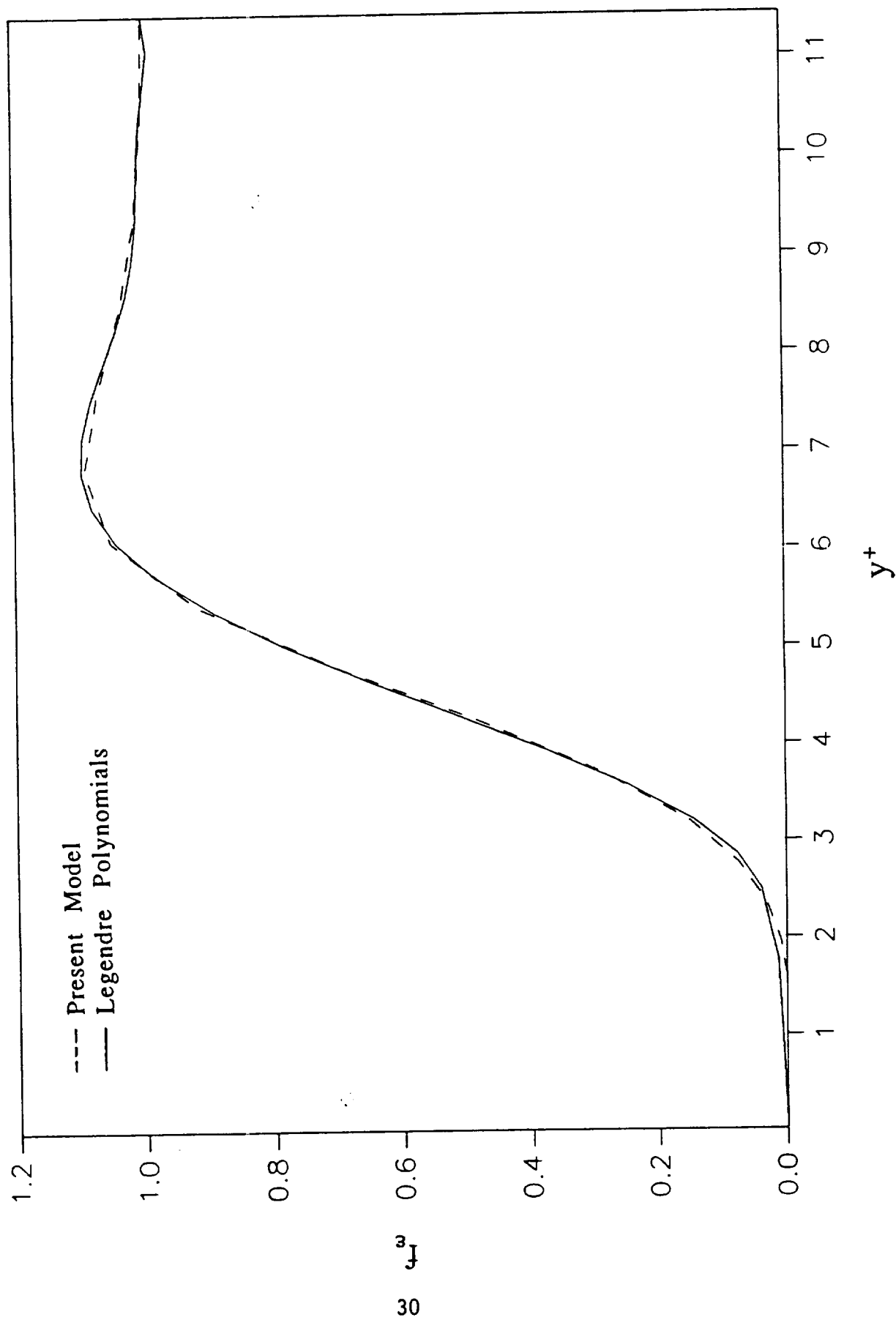Figure 9   The budget of k in the near-wall region.

29

Figure 10 A curve fit to the dissipation damping function in the near-wall region.

30